

ISSN: 2576-8840





Theoretical Investigation on Brønsted-Base-Catalyzed Diversified Annulations of Ethylidene 1,3-Indenedione and Vinyl 1,2-Diketone Delivering Oxabicyclo[3.2.1] Octane, Spiro[4.5] Decane, and Branched Triquinane

Nan Lu* and Chengxia Miao

College of Chemistry and Material Science, Shandong Agricultural University, P. R. China

*Corresponding author: Nan Lu, College of Chemistry and Material Science, Shandong Agricultural University, Taian 271018, P. R. China

Submission:  July 29, 2024
Published:  August 08, 2024

Volume 20 - Issue 4

How to cite this article: Nan Lu* and Chengxia Miao. Theoretical Investigation on Brønsted-Base-Catalyzed Diversified Annulations of Ethylidene 1,3-Indenedione and Vinyl 1,2-Diketone Delivering Oxabicyclo[3.2.1]Octane, Spiro[4.5] Decane, and Branched Triquinane. *Res Dev Material Sci.* 20(4). RDMS. 000993. 2024. DOI: [10.31031/RDMS.2024.20.000993](https://doi.org/10.31031/RDMS.2024.20.000993)

Copyright@ Nan Lu, This article is distributed under the terms of the Creative Commons Attribution 4.0 International License, which permits unrestricted use and redistribution provided that the original author and source are credited.

Abstract

Our DFT calculations provide the first theoretical investigation on Brønsted-base-catalyzed annulation of ethylidene 1,3-indenedione with vinyl 1,2-diketone. After Michael addition between deprotonated ethylidene 1,3-indenedione and vinyl 1,2-diketone, three paths are possible. In path A, intramolecular oxa-Michael addition and proton transfer happen at first followed by intramolecular aldol reaction furnishing oxabicyclo [3.2.1] octane after protonation. In path B, the oxygen heterocyclic rings of deprotonated oxabicyclo [3.2.1] octane are destructed simultaneously through primary complicated ring opening. The ring expansion proceeds via intramolecular aldol reaction followed by readily proton transfer. The intramolecular annulation splits eight membered ring into two five membered ones for branched triquinane. In path C, after proton transfer, intramolecular aldol reaction provides hexacyclic alkene for spiro [4.5] decane. The positive solvation effect is suggested by decreased absolute and activation energies in solution compared with in gas. These results are supported by Multiwfn analysis on FMO composition of specific TSs, and MBO value of vital bonding, breaking.

Keywords: Brønsted-base; Polycyclic; 1,3-indenedione; Intramolecular aldol reaction; Michael addition

Introduction

The complicated 3-dimensional molecular skeletons are active substances biologically and exist widely in natural products. As major targets of organic synthesis, the rapid and concise construction has received much interest especially three key types still challenging starting from same substrates. For example, oxabicyclo[3.2.1]-octane was obtained from acid-promoted aromatization rearrangement with antiprotozoal activity [1,2]. The spiro[4.5] decane was known to function as potent, selective, and efficacious β -secretase (BACE1) inhibitor for prevention of alzheimer's disease [3,4]. The branched triquinane was achieved via supramolecular catalysis leonidas-dimitrios syntrivanis [5,6]. The ethylidene 1,3-indenedione (EID) was versatile to develop new reaction modes accessing the above natural skeletons and thus is desirable in organic synthesis. Recent progresses are annulation with reagents

involving both electrophilic and nucleophilic properties forming bicyclic products [7], affording spirocyclic compounds via proton transfer [8-10] or vinylogous type nucleophilic addition [11].

On the other hand, much interest has been focused on exploring novel reactions of 1,2-diketone. Yang reported construction of dispiro-indenone via domino cycloaddition of α,β -unsaturated aldimines with 2-arylidene-1,3-indenediones and 2,2'-(arylmethylene)bis(1,3-indenediones) [12]. Huang achieved synthesis of 7'-arylidenespiro [indoline-3,1'-pyrrolizines] and 7'-arylidenespiro[indene-2,1'-pyrrolizines] via [3 + 2] cycloaddition and β -C-H functionalized pyrrolidine [13]. Kong obtained chemodivergent annulations or copper-catalyzed diversified version between α -diketones and alkynyl α -diketones [14,15]. Chen got dihydrofuranones via oxa-nazarov cyclization-Michael addition sequence [16]. Then Chen reported dynamic kinetic resolution of β -substituted α -diketones via asymmetric transfer hydrogenation [17]. Cao achieved asymmetric deoxygenative cyclopropanation by chiral salen-Mo catalyst [18]. There were typical outcome about Tian's catalytic enantioselective biltz synthesis [19], Chen's organocatalytic enantioselective synthesis of axially chiral N,N'-bisindoles [20], Luo's tandem cyclization/hydrosilylation towards enantio- and diastereoselective construction of trans-2,3-disubstituted-1,2,3,4-tetrahydroquinoxalines catalyzed by borane [21], and Tian's diastereo- and enantioselective oxa-Nazarov cyclization-Michael addition of conjugated 1,2-diketones under asymmetric binary-acid catalysis [22]. Thus, the rapid construction of complicated molecules is very attractive through regio- and stereoselective transformations.

As far as we know, the development in recent years was few besides multicomponent cyclizative 1,2-rearrangement enabled enantioselective construction of 2,2-disubstituted pyrrolinones of Li group and asymmetric transfer hydrogenation of cyclobutenediones by Lan [23,24]. Considering the merits of aforementioned two substrates, a breakthrough was Liu's Brønsted-base-catalyzed annulations between ethylidene 1,3-indenedione and vinyl 1,2-diketone [25]. Via modification of reaction conditions, three types of thoroughly different polycyclic skeletons were obtained and two unprecedented reaction modes were predicted. Although oxabicyclo[3.2.1]octane, spiro[4.5]decane, and branched triquinane were yielded, many problems still puzzled and there was no report about detailed mechanistic study explaining potential of 1,2-diketone. What is the vital role of base in controlling different products? Why weaker base favors stable enolate and finally affords spiro[4.5]decane while stronger one facilitating oxa-Michael to produce oxabicyclo[3.2.1]octane? How controversial resonance structures reasonably exist or be excluded in specific process? To solve these questions in experiment, an in-depth theoretical study was necessary for this strategy focusing on the competition of three possible paths, unique reactivity of EID and origin of product diversity.

Computational Details

Optimized structures were obtained at M06-2X/6-31G(d) level

of theory with GAUSSIAN09 [26]. In tests of popular DFT methods [27], M06-2X functional attained smaller standard deviation of difference between calculated value and experimental value in geometries than B3LYP including Becke's three-parameter hybrid functional combined with Lee-Yang-Parr correction for correlation [28,29]. The best compromise between accuracy and time consumption was provided with 6-31G(d) basis set on energy calculations. Also, M06-2X functional was found to give relatively accurate results for catalysed enantioselective (4 + 3), concerted [4 + 2], stepwise (2 + 2) cycloaddition and catalysed Diels-Alder reactions [30,31]. Together with the best performance on noncovalent interaction, M06-2X functional is believed to be suitable for this system [32-34]. The nature of each structure was verified by performing harmonic vibrational frequency calculations. Intrinsic Reaction Coordinate (IRC) calculations were examined to confirm the right connections among key transition-states and corresponding reactants and products. Harmonic frequency calculations were carried out at the M06-2X/6-31G(d) level to gain zero-point vibrational energy (ZPVE) and thermodynamic corrections at 298 K and 1 atm for each structure in 1,4-dioxane.

The solvation-corrected free energies were obtained at the M06-2X/6-311++G(d,p) level by using integral equation formalism polarizable continuum model (IEFPCM) in Truhlar's "density" solvation model [35-39] on the M06-2X/6-31G(d)-optimized geometries. As an efficient method obtaining bond and lone pair of a molecule from modern ab initio wave functions, NBO procedure was performed with Natural bond orbital (NBO3.1) to characterize electronic properties and bonding orbital interactions [40-42]. The wave function analysis was provided using Multiwfn_3.7_dev package [43] including research on Frontier Molecular Orbital (FMO) and Mayer Bond Order (MBO).

Results and Discussion

The mechanism was explored for Brønsted-base-catalyzed annulation of ethylidene 1,3-indenedione 1 with vinyl 1,2-diketone 2 leading to oxabicyclo[3.2.1]octane 3, branched triquinane 4, spiro[4.5]decane 5 (Figure 1). Illustrated by black arrow of Scheme 2, 1 is deprotonated by base to afford dienolate, which attacks 2 through Michael addition producing i2. Starting from i2, three paths are possible. In path A, an intramolecular oxa-Michael addition happens to form i3 and after proton transfer to generate i4. From the resonated enolate structure of i4, an intramolecular aldol reaction occurs furnishing i5, which provides 3 after protonation (red arrow). In path B, 3 is able to undergo deprotonation at another site to give i6 and after ring opening to generate i7, which proceeds intramolecular aldol reaction to achieve further ring expansion of i8. After proton transfer, i8 turns to be i9, the resonance structure of which undergoes intramolecular annulation affording i10. 4 is produced from the protonation of i10 (blue arrow). In path C, the proton transfer from i2 yields i11, a resonance structure of which becomes more stable via isomerization leading to i12. Then an intramolecular aldol reaction occurs providing i13. 5 is obtained after protonation of i13 (green arrow). The schematic structures

of optimized TSs in Figure 2 were listed by Figure 3. The activation energy was shown in Table 1 for all steps. Supplementary Table 2, Table 3 provided the relative energies of all stationary points.

According to experiment, the Gibbs free energies in 1,4-dioxane solution phase are discussed here.

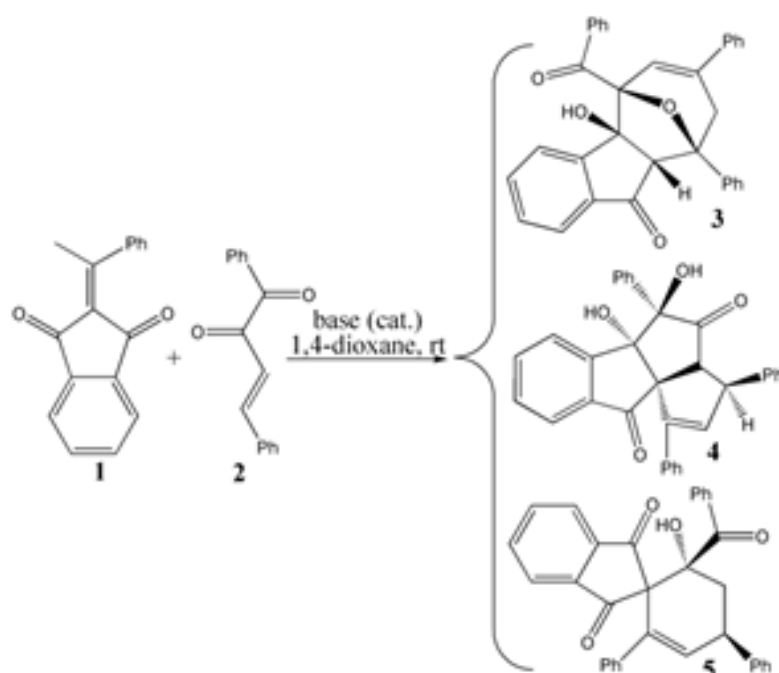


Figure 1: Brønsted-base-catalyzed annulation of ethylidene 1,3-indenedione 1 with vinyl 1,2-diketone 2 leading to oxabicyclo[3.2.1]octane 3, branched triquinane 4, spiro[4.5]decane 5.

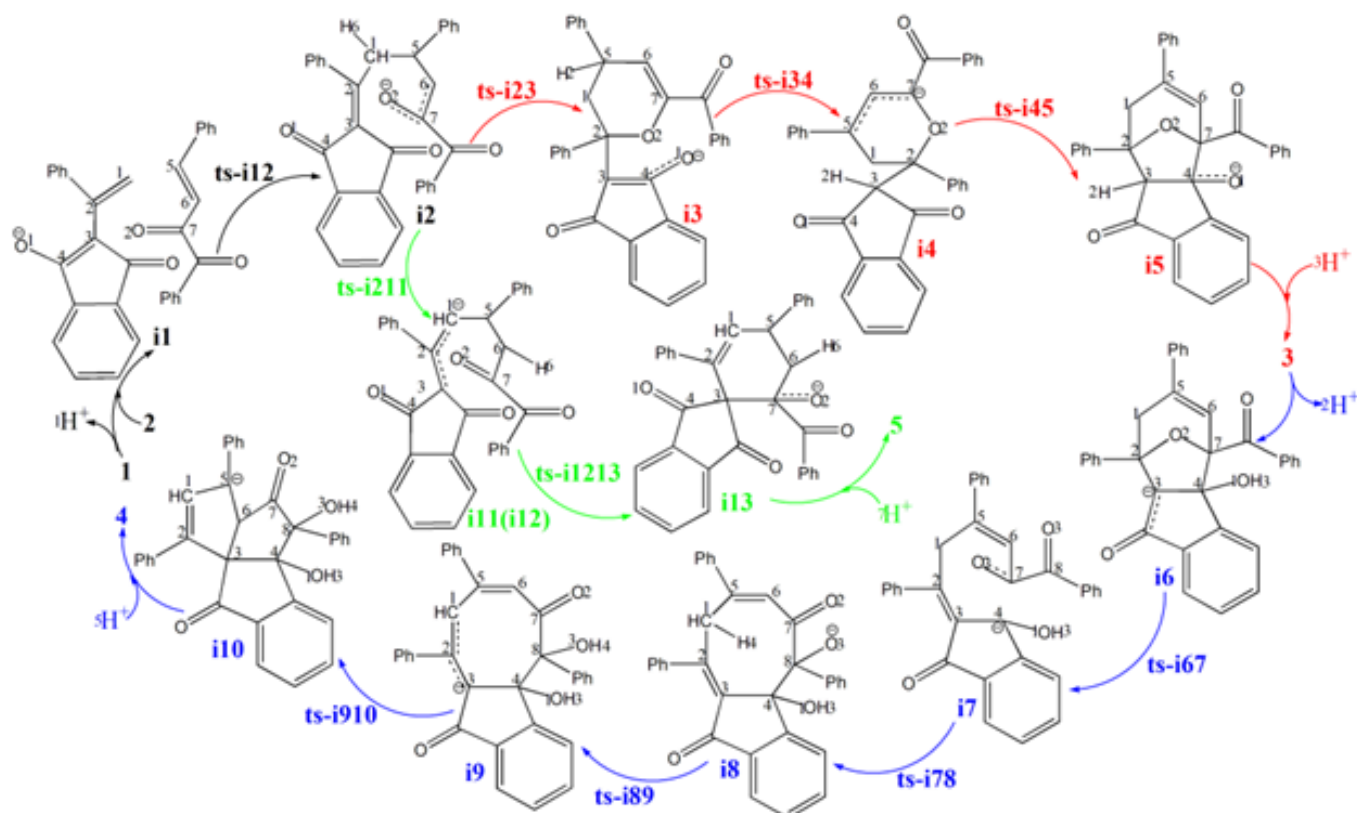


Figure 2: Proposed reaction mechanism of Brønsted-base-catalyzed annulation of 1 with 2 leading to 3, 4, 5. TS is named according to the two intermediates it connects.

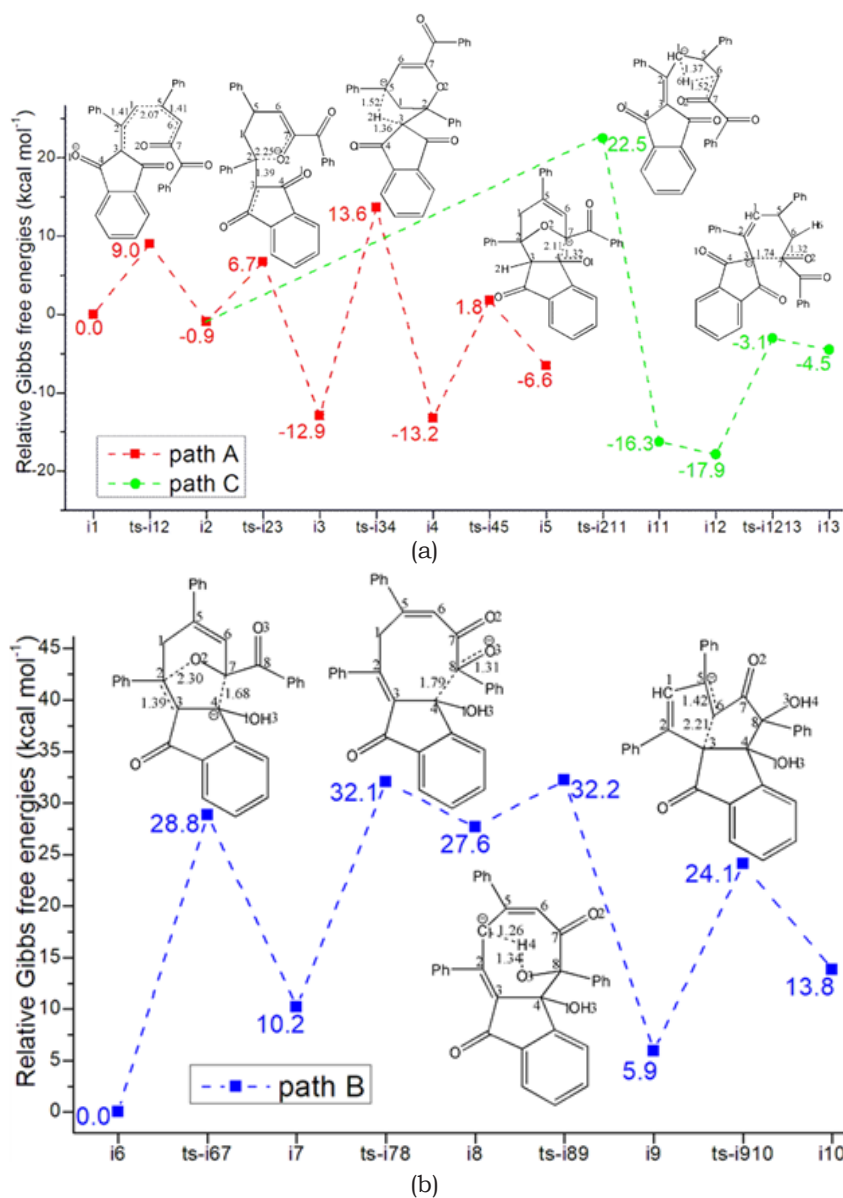


Figure 3: Proposed reaction mechanism of Brønsted-base-catalyzed annulation of 1 with 2 leading to 3, 4, 5. TS is named according to the two intermediates it connects.

Table 1: The activation energy (in kcal mol⁻¹) of all reactions in gas and solvent.

	$\Delta G_{\text{gas}}^{\ddagger}$	$\Delta G_{\text{sol}}^{\ddagger}$
ts-i12	8.1	9.0
ts-i23	6.1	7.6
ts-i34	26.7	26.5
ts-i45	15.3	15.0
ts-i67	31.2	28.8
ts-i78	23.9	21.9
ts-i89	4.2	4.6
ts-i910	17.0	18.2
ts-i211	26.0	23.4
ts-i1213	20.4	14.8

Table 2: Calculated relative energies (all in kcal mol⁻¹, relative to isolated species) for the ZPE-corrected Gibbs free energies (ΔG_{gas}), Gibbs free energies for all species in solution phase (ΔG_{sol}) at 298K by M06-2X/6-311++G(d,p)//M06-2X/6-31G(d) method and difference between absolute energy.

Species	ΔG_{gas}	$\Delta G_{\text{sol(1,4-dioxane)}}$
1+2-h	0.00	0.00
i1	8.03	-11.16
ts-i12	16.15	-2.18
i2	10.40	-12.10
ts-i23	16.50	-4.46
i3	-3.33	-24.11
ts-i34	23.41	2.47
i4	-0.86	-24.38
ts-i45	14.47	-9.40
i5	6.65	-17.73
i6	9.50	-12.52
ts-i67	40.68	16.29
i7	19.74	-2.31
ts-i78	43.66	19.54
i8	36.27	15.11
ts-i89	40.44	19.68
i9	13.67	-6.59
ts-i910	30.69	11.61
i10	24.09	1.31
ts-i211	36.44	11.30
i11	-3.32	-27.41
i12	-7.06	-29.02
ts-i1213	13.29	-14.22
i13	9.16	-15.65
1+2	0.00	0.00
3	-34.15	-35.53
4	-18.40	-25.32
5	-28.54	-32.45

Table 3: The activation energy (local barrier) (in kcal mol⁻¹) of all reactions in the gas, solution phase calculated with M06-2X/6-311++G(d,p)//M06-2X/6-31G(d) method.

TS	$\Delta G_{\text{gas}}^{\ddagger}$	$\Delta G_{\text{sol}}^{\ddagger}$
ts-i12 (342i)	8.1	9.0
ts-i23 (95i)	6.1	7.6
ts-i34 (385i)	26.7	26.5
ts-i45 (106i)	15.3	15.0
ts-i67 (162i)	31.2	28.8
ts-i78 (84i)	23.9	21.9
ts-i89 (1045i)	4.2	4.6
ts-i910 (298i)	17.0	18.2
ts-i211 (527i)	26.0	23.4
ts-i1213 (108i)	20.4	14.8

**Michael addition/intramolecular oxa-Michael addition/
proton transfer/intramolecular aldol reaction**

Initially the complex denoted as i1 is located between

deprotonated 1 and 2. Michael addition proceeds via ts-i12 in step 1 with the activation energy of 9.0 kcal mol⁻¹ relative to the starting point i1 exothermic by -0.9 kcal mol⁻¹ producing i2 (red dash line

of Figure 3a). The transition vector includes nucleophilic attack of negative C1 to positive C5, and the cooperated stretching of C1-C2, C5-C6 double bond to single one almost the same (2.07, 1.41,

1.41 Å) (Figure 4a). The linkage of C1-C5 in i2 not only makes C1 changing from sp² hybrid to sp³ but transfers the negative charge to O2 as a preparation of next step.

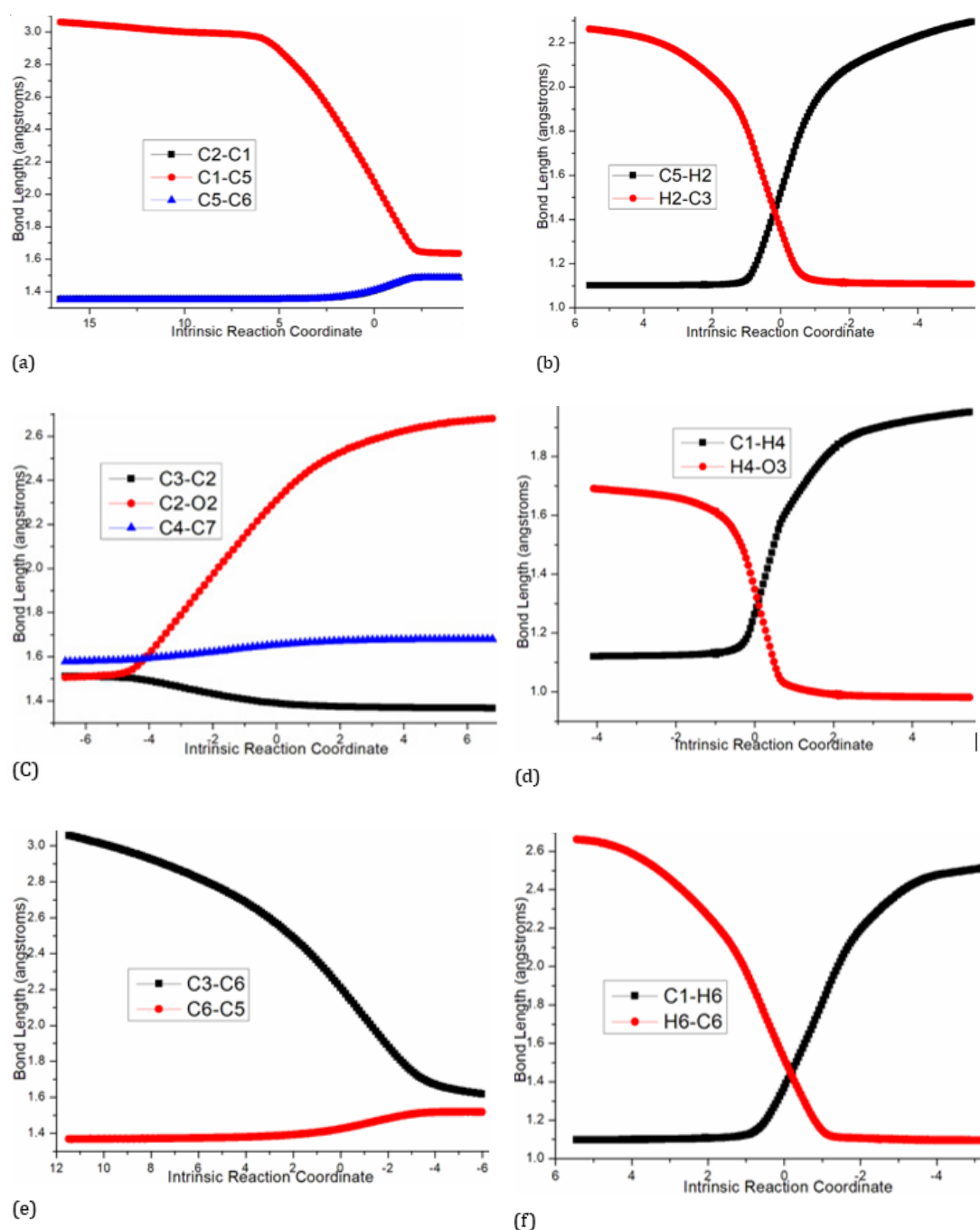


Figure 4: Evolution of bond lengths along the IRC for (a) ts-i12 (b) ts-i34 (c) ts-i67 (d) ts-i89 (e) ts-i910 (f) ts-i211 at M06-2X/6-311++G(d,p) level

In path A, an intramolecular oxa-Michael addition occurs via ts-i23 as step 2 with activation energy of 7.6 kcal mol⁻¹ exothermic by -12.9 kcal mol⁻¹ giving stable i3. The transition vector contains nucleophilic addition of negative O2 to positive C2 and the corresponding C2-C3 double bond elongated to single one

(2.25, 1.39 Å). C2 turns to be sp³ hybrid in resultant i3 with new oxygenated hexagonal ring, in which O1 recovers to be anion.

Then the proton transfer takes place via ts-i34 in subsequent step 3 with activation energy of 26.5 kcal mol⁻¹ affording i4 exothermic by -13.2 kcal mol⁻¹. According to the transition vector,

the proton H2 is transferring from C5 to C3 making C3 sp³ hybrid and the double bond on C3-C4 moving to C4-O1 carbonyl group (1.52, 1.36 Å) (Figure 4b). The negative charge is shared by delocalized π bond on C5-C6-C7, which enhance the nucleophilic ability of C7 favorable for next step.

In next step 4 from the resonated enolate structure of i4, an intramolecular aldol reaction occurs via ts-i45 with activation energy of 15.0 kcal mol⁻¹ exothermic by -6.6 kcal mol⁻¹ delivering intermediate i5. The transition vector corresponds to the approaching of C7 to C4 and elongation of C4-O1 bond from double to single (2.11, 1.32 Å). Once C7-C4 is bonded, a new oxygen-containing five membered ring is available forming the vital structure of product oxabicyclo[3.2.1]octane 3, which is provided after addition of one proton on negative O1 of i5. Ultimately, the proton transfer in step 3 is determined to be rate-limiting for path A.

Ring opening/intramolecular aldol reaction/proton transfer/intramolecular annulation

3 is taken as precursor for path B (blue dash line of Figure 3b), from which the deprotonation of H2 on C3 gives stable i6 as new starting point of step 1. This complicated ring opening happens via ts-i67 with activation energy of 28.8 kcal mol⁻¹ endothermic by 10.2 kcal mol⁻¹ generating intermediate i7. The transition vector reveals detailed atomic motion comprising shortened C2-C3 single bond to double, the cleavage of C2-O2 and C4-C7 as well as slightly strengthened C7-O2 (1.39, 2.30, 1.68 Å) (Figure 4c). Evidently, the transfer of negative charge on C3 to C2-C3 promotes double bond formation, dissociation from O2 to C2 and further triggers fracture from C7 to C4. Here the oxygen heterocyclic rings of 3 are destructed simultaneously getting ready for the formation of new product.

Subsequently, the negative C4 attacks another adjacent positive carbonyl C8 in an intramolecular aldol mode via ts-i78 in step 2 with activation energy of 21.9 kcal mol⁻¹ yielding i8 endothermic by 27.6 kcal mol⁻¹. This process is illustrated according to the transition vector composed of C4...C8 bonding and C8...O3 extension (1.79, 1.31 Å). Besides weakened C8-O3 to single one, the structure of i8 is expanded into a loose eight membered ring involving negatively charged O3 conducive to accept proton.

Therefore, the following proton transfer is easy via ts-i89 with a low barrier of only 4.6 kcal mol⁻¹ endothermic by 5.9 kcal mol⁻¹ giving i9 in step 3. The relative energy of i9 is decreased by 21.7 kcal mol⁻¹ from that of former i8 quite favorable thermodynamically yet still reactive to initiate next step. The proton H4 is shifting from sp³ hybridized C1 to negatively charged O3 seen from the detailed

motion demonstrated by the transition vector (1.26, 1.34 Å) (Figure 4d). Like the case of i4, the negative charge on C1 of i9 is shared with C3 via delocalized C1-C2-C3 π bond in its resonance structure, which readily initiates next nucleophilic attack.

In step 4, the intramolecular annulation is completed via ts-i910 with mediate activation energy of 18.2 kcal mol⁻¹ endothermic by 13.8 kcal mol⁻¹ producing another vital precursor i10. The transition vector is about nucleophilic attack of C3 to C6 and concerted elongation of C6-C5 bond from double to single (2.21, 1.42 Å) (Figure 4e). Consequently, the eight membered ring is splited into two five membered rings sharing newly formed C3-C6 single bond that is the formation of product branched triquinane 4 after protonation on negatively charged C5. Obviously, the complicated ring opening of step 1 is determined to be rate-limiting for path B.

Proton transfer/intramolecular aldol reaction

In addition to oxa-Michael addition, there is feasible proton transfer existing from i2 via ts-i211 as step 1 of path C (green dash line of Figure 3a). The activation energy is 23.4 kcal mol⁻¹ exothermic by -16.3 kcal mol⁻¹ yielding i11. The transition vector corresponds to proton H6 transferring from sp³ hybridized C1 to negative C6 (1.37, 1.52 Å) (Figure 4f). The same as i9, the negative charge on C1 is also shared by C3 in the resonance structure of i11, which further isomerizes to more stable i12.

Different from the case of path A and B aforementioned, C3 attacks positive carbonyl C7 in an intramolecular aldol reaction via ts-i1213 with activation energy of 14.8 kcal mol⁻¹ exothermic by -4.5 kcal mol⁻¹ in step 2. Thus C7-O2 double bond is weakened to single one with negatively charged O2 in i13 characterized by newly formed hexacyclic alkene. The product spiro[4.5]decane 5 is obtained after protonation on O2. The proton transfer in step 1 is determined to be rate-limiting for path C.

From kinetics, path B is inferior to another two competitive paths. Furthermore, the relative energy of all stationary points are comparatively high and is not advantageous from the perspective of entire potential energy surface. Hence the products 3 and 5 are proposed to be superior to 4 not only from the stability of themselves but from their precursors i5, i13 and i10. To highlight the idea of feasibility for changes in electron density and not molecular orbital interactions are responsible of the reactivity of organic molecules, quantum chemical tool Multiwfn was applied to analyze of electron density such as MBO results of bonding atoms and contribution of atomic orbital to HOMO of typical TSs (Table 4, Figure 5). These results all confirm the above analysis.

Table 4: Mayer bond order (MBO) of typical TSs.

	C2...C1	C1...C5	C5...C6
ts-i12			
1.37	0.43	1.30	
	O2...C2	C2...C3	
ts-i23	0.26	1.47	
	C5...H2	H2...C3	

ts-i34	0.38	0.48	
	C7...C4	C4...O1	
ts-i45	0.58	1.26	
	C3...C2	C2...O2	C7...C4
ts-i67	1.51	0.20	0.82
	C4...C8	C8...O3	
ts-i78	0.66	1.27	
	C6...H5	H5...O4	
ts-i89	0.52	0.29	
	C3...C6	C6...C5	
ts-i910	0.44	1.25	
	C1...H6	H6...C6	
ts-i211	0.47	0.38	
	C3...C7	C7...O2	
ts-i1213	0.77	1.21	

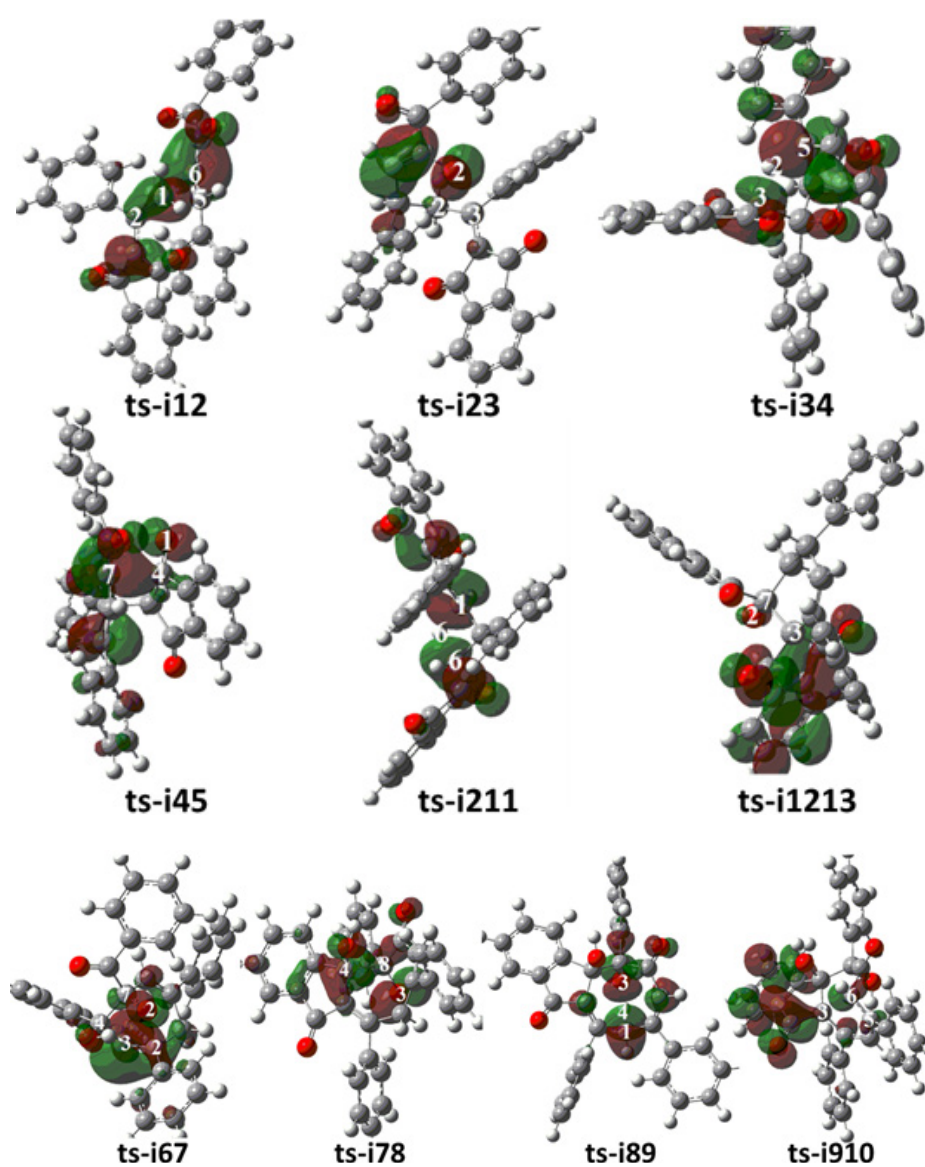


Figure 5: Highest Occupied Molecular Orbital (HOMO) of typical TSs. Different colors are used to identify the phase of the wave functions

Conclusion

Our DFT calculations provide the first theoretical investigation on Brønsted-base-catalyzed annulation of ethylidene 1,3-indenedione with vinyl 1,2-diketone. The deprotonated ethylidene 1,3-indenedione attacks vinyl 1,2-diketone via Michael addition. Then three paths are possible. In path A, an intramolecular oxa-Michael addition and proton transfer happen at first giving enolate. From the resonated structure, an intramolecular aldol reaction occurs furnishing product oxabicyclo[3.2.1]octane after protonation. The path B is initiated by deprotonation of oxabicyclo[3.2.1]octane at another site. The oxygen heterocyclic rings are destructed simultaneously after primary ring opening. Then ring expansion is achieved via intramolecular aldol reaction followed by readily proton transfer. The intramolecular annulation occurs splitting loose eight membered ring into two five membered rings for branched triquinane. In path C, after proton transfer, an intramolecular aldol reaction occurs providing newly formed hexacyclic alkene for spiro[4.5]decane. The proton transfer is determined to be rate-limiting for path A and C whereas ring opening for path B. The path B is inferior to path A and C not only from activation energy but from relative energy of all stationary points on potential energy surface. The positive solvation effect is suggested by decreased absolute and activation energies in 1,4-dioxane solution compared with in gas. These results are supported by Multiwfn analysis on FMO composition of specific TSs, and MBO value of vital bonding, breaking.

References

- Farimani MM, Khodaei B, Moradi H, Aliabadi A, Ebrahimi SN, et al. (2018) Phytochemical study of *Salvia leucifolia* roots: Rearranged abietane diterpenoids with antiprotozoal activity. *J Nat Prod* 81: 1384-1390.
- Li Y, Li G, Dong Y, Ma X, Dong H, et al. (2019) Orobanone analogues from acid-promoted aromatization rearrangement of curcuminol inhibit hypoxia-inducible factor-1 (HIF-1) in cell-based reporter assays. *Bioorg Chem* 85: 357-363.
- Machauer R, Lueoend R, Hurth K, Veenstra SJ, Rueeger H, et al. (2021) Discovery of umibecestat (CNP520): A potent, selective, and efficacious β -secretase (BACE1) inhibitor for the prevention of Alzheimer's disease. *J Med Chem* 64: 15262-15279.
- Cox RJ, McCreanor NG, Morrison JA, Munday RH, Taylor BA (2023) Copper-catalyzed racemization-recycle of a quaternary center and optimization using a combined kinetics-DoE/MLR modeling approach. *J Org Chem* 88: 5275-5284.
- Wang Y, Yu ZX (2015) Rhodium-catalyzed [5 + 2 + 1] cycloaddition of enevinylcyclopropanes and CO: Reaction design, development, application in natural product synthesis, and inspiration for developing new reactions for synthesis of eight-membered carbocycles. *Acc Chem Res* 48: 2288-2296.
- Némethová I, Schmid D, Levi S, Prescimone A, Bissegger F, et al. (2020) Four-step access to the sesquiterpene natural product presilphiperfolan-1 β -ol and unnatural derivatives via supramolecular catalysis leonidas-dimitrios syntrivannis. *J Am Chem Soc* 142: 5894-5900.
- Möhlmann L, Chang GH, Reddy GM, Lee CJ, Lin W (2016) Organocatalytic enantioselective synthesis of tetrahydrofluoren-9-ones via vinylogous Michael addition/henry reaction cascade of 1,3-indandione-derived pronucleophiles. *Org Lett* 18: 688-691.
- Gao Y, Liu D, Fu Z, Huang W (2019) Facile synthesis of 2,2-diacyl spirocyclohexanones via an N-heterocyclic carbene-catalyzed formal [3C + 3C] annulation. *Org Lett* 21: 926-930.
- Wang M, Tseng PY, Chi WJ, Suresh S, Edukondalu A, et al. (2020) Diversity-oriented synthesis of spirocyclo-hexene indane-1,3-diones and coumarin-fused cyclopentanes via an organobase-controlled cascade reaction. *Adv Synth Catal* 362: 3407-3415.
- Kuan JY, Chen IT, Lin H, Han JL (2023) Organocatalytic vinylogous Michael addition/cyclization cascade of 2-alkylidene indane-1,3-diones with enals: A regio- and stereo-controlled diversity-oriented route to indane-1,3-dione derivatives. *Adv Synth Catal* 365: 3493-3504.
- Chen IT, Guan RY, Han JL (2022) Asymmetric sequential vinylogous Mannich/annulation/acylation process of 2-ethylidene 1,3-indandiones and isatin N-Boc ketimines: Access to chiral spiro-oxindole piperidine derivatives. *Adv Synth Catal* 364: 2613-2619.
- Yang WJ, Fang HL, Sun J, Yan CG (2019) Construction of dispiro-indenone scaffolds via domino cycloaddition reactions of α,β -unsaturated aldimines with 2-arylidene-1,3-indenediones and 2,2'-(Arylmethylene) bis(1,3-indenediones). *ACS Omega* 4: 13553-13569.
- Huang Y, Fang HL, Huang YX, Sun J, Yan CG (2019) Synthesis of 7'-arylidenespiro [indoline-3,1'-pyrrolizines] and 7'-arylidenespiro[indene-2,1'-pyrrolizines] via [3 + 2] cycloaddition and β -C-H functionalized pyrrolidine. *J Org Chem* 84: 12437-12451.
- Kong X, Yu F, Chen Z, Gong F, Yang S, et al. (2021) Catalytic chemodivergent annulations between α -diketones and alkynyl α -diketones. *Sci China Chem* 64: 991-998.
- Kong X, Yu F, Niu S, Gong F, Yang S, et al. (2022) Copper-catalyzed diversified annulations between α -diketones and alkynyl α -diketones. *Chin Chem Lett* 33: 2997-3002.
- Chen T, Gong F, Nagaraju S, Liu J, Yang S, et al. (2022) Oxa-nazarov cyclization-michael addition sequence for the rapid construction of dihydrofuranones. *Org Lett* 24: 8837-8842.
- Chen T, Liu W, Gu W, Niu S, Lan S, et al. (2023) Dynamic kinetic resolution of β -substituted α -diketones via asymmetric transfer hydrogenation. *J Am Chem Soc* 145: 585-599.
- Cao LY, Wang JL, Wang K, Wu JB, Wang DK, et al. (2023) Catalytic asymmetric deoxygenative cyclopropanation reactions by a chiral salen-mo catalyst. *J Am Chem Soc* 145: 2765-2772.
- Tian D, Li ZC, Sun ZH, He YP, Xu LP, et al. (2023) Catalytic enantioselective biltz synthesis. *Angew Chem Int Ed* 62: e202313797.
- Chen ZH, Li TZ, Wang NY, Ma XF, Ni SF, et al. (2023) Organocatalytic enantioselective synthesis of axially chiral N,N'-bisindoles. *Angew Chem Int Ed* 62: e202300419.
- Luo Z, Li Z, Zhao H, Yang J, Xu L, et al. (2023) Borane-catalyzed tandem cyclization/hydrosilylation towards enantio- and diastereoselective construction of trans-2,3-disubstituted-1,2,3,4-tetrahydroquinoxalines. *Angew Chem Int Ed* 62: e202305449.
- Tian Y, Tang M, Lian C, Song R, Yang D, et al. (2023) Asymmetric binary-acid catalysis: a diastereo- and enantioselective oxa-nazarov cyclization-michael addition of conjugated 1,2-diketones. *Org Chem Front* 10: 3039-3044.
- Li XZ, He YP, Wu H (2024) Multicomponent cyclizative 1,2-rearrangement enabled enantioselective construction of 2,2-disubstituted pyrrolinones. *Angew Chem Int Ed* 63: e202317182.
- Lan S, Huang H, Liu W, Xu C, Lei X, et al. (2024) Asymmetric transfer hydrogenation of cyclobutenediones. *J Am Chem Soc* 146: 4942-4957.
- Zhu L, Luo H, Liu J, Luo B, Yang S, et al. (2024) Rapid construction of polycyclic skeletons via Brønsted-base-catalyzed annulations of ethylidene 1,3-indenediones and vinyl 1,2-diketones. *Org Lett* 26(28): 5893-5898.
- Frisch MJ, Trucks GW, Schlegel HB, et al. (2010) Gaussian 09 (Revision B.01), Gaussian, Inc., Wallingford, CT.
- Stephens PJ, Devlin FJ, Chabalowski CF, Frisch MJ (1994) Ab initio calculation of vibrational absorption and circular dichroism spectra using density functional force fields. *J Phys Chem* 98: 11623-11627.

28. Becke AD (1996) Density-functional thermochemistry. IV. A new dynamical correlation functional and implications for exact-exchange mixing. *J Chem Phys* 104: 1040-1046.
29. Lee CT, Yang WT, Parr RG (1988) Development of the colle-salvetti correlation-energy formula into a functional of the electron density. *Phys Rev B* 37: 785-789.
30. Li X, Kong X, Yang S, Meng M, Zhan X, et al. (2019) Bifunctional thiourea-catalyzed asymmetric inverse-electron-demand diels-alder reaction of allyl ketones and vinyl 1,2-diketones via dienolate intermediate. *Org Lett* 21: 1979-1983.
31. Krenske EH, Houk KN, Harmata M (2015) Computational analysis of the stereochemical outcome in the imidazolidinone-catalyzed enantioselective (4 + 3)-cycloaddition reaction. *J Org Chem* 80: 744-750.
32. Lv H, Han F, Wang N, Lu N, Song Z, et al. (2022) Ionic liquid catalyzed c-c bond formation for the synthesis of polysubstituted olefins. *Eur J Org Chem* 2022: e202201222.
33. Zhuang H, Lu N, Ji N, Han F, Miao C (2021) Bu₄NHSO₄-catalyzed direct n-allylation of pyrazole and its derivatives with allylic alcohols in water: A metal-free, recyclable and sustainable system. *Advanced Synthesis & Catalysis* 363: 5461-5472.
34. Lu N, Liang H, Qian P, Lan X, Miao C (2020) Theoretical investigation on the mechanism and enantioselectivity of organocatalytic asymmetric Povarov reactions of anilines and aldehydes. *Int J Quantum Chem* 120: e26574.
35. Tapia O (1992) Solvent effect theories: Quantum and classical formalisms and their applications in chemistry and biochemistry. *J Math Chem* 10: 139-181.
36. Tomasi J, Persico M (1994) Molecular interactions in solution: an overview of methods based on continuous distributions of the solvent. *Chem Rev* 94: 2027-2094.
37. Simkin BY, Shekhet I (1995) Quantum chemical and statistical theory of solutions-A computational approach. Ellis Horwood, London.
38. Tomasi J, Mennucci B, Cammi R (2005) Quantum mechanical continuum solvation models. *Chem Rev* 105: 2999-3093.
39. Marenich AV, Cramer CJ, Truhlar DG (2009) Universal solvation model based on solute electron density and on a continuum model of the solvent defined by the bulk dielectric constant and atomic surface tensions. *J Phys Chem B* 113: 6378-6396.
40. Reed AE, Weinstock RB, Weinhold F (1985) Natural population analysis. *J Chem Phys* 83: 735-746.
41. Reed AE, Curtiss LA, Weinhold F (1988) Intermolecular interactions from a natural bond orbital donor-acceptor view point. *Chem Rev* 88: 899-926.
42. Foresman JB, Frisch A (1996) Exploring chemistry with electronic structure methods, (2nd edn), Gaussian, Inc., Pittsburgh, USA.
43. Lu T, Chen F (2012) Multiwfn: A multifunctional wavefunction analyzer. *J Comput Chem* 33: 580-592.